Protein Tags

How to cite:
International Edition: doi.org/10.1002/anie.202207905
German Edition: doi.org/10.1002/ange.202207905

Third-Generation Covalent TMP-Tag for Fast Labeling and Multiplexed Imaging of Cellular Proteins

*Jiaming Mo[+], Jingting Chen[+], Yabo Shi, Jingfu Sun, Yunxiang Wu, Tianyan Liu, Junwei Zhang, Yu Zheng, Yulong Li, and Zhixing Chen**

Abstract: Self-labeling protein tags can introduce advanced molecular motifs to specific cellular proteins. Here we introduce the third-generation covalent TMP-tag (TMP-tag3) and showcase its comparison with HaloTag and SNAP-tag. TMP-tag3 is based on a proximity-induced covalent Michael addition between an engineered Cys of E. coli dihydrofolate reductase (eDHFR) and optimized trimethoprim (TMP)–acrylamide conjugates with minimal linkers. Compared to previous versions, the TMP-tag3 features an enhanced permeability when conjugated to fluorogenic spirocyclic rhodamines. As a small protein, the 18-kD eDHFR is advantageous in tagging selected mitochondrial proteins which are less compatible with bulkier HaloTag fusions. The proximal N–C termini of eDHFR also enable facile insertion into various protein loops. TMP-tag3, HaloTag, and SNAP-tag are orthogonal to each other, collectively forming a toolbox for multiplexed live-cell imaging of cellular proteins under fluorescence nanoscopy.

Introduction

Introducing new functions to biomacromolecules has been a central theme of bioconjugation chemistry. A particular focus of this decade has been to do so in live cells and organisms. Along this line, chemists have accumulated a diverse toolkit for coupling small molecules to proteins of interest.[1,2] From a chemistry point of view, a protein tag could be as small as a single reactive unnatural amino acid,[3,4] or a short peptide.[5] Although these tags are useful in precisely labeling and manipulating proteins,[6] they require the deliberate expression of excessive supplementary enzymes to guarantee reactivity and selectivity. On the other side of the spectrum, self-labeling tags require only a simple fusion with proteins of interest, followed by the labeling of a small molecule that can specifically recognize the tag and react without undergoing other enzymatic processes. Since the conception of the seminal FlAsH tag in 1998,[7] a handful of self-labeling tags have been developed, including the FlAsH/ReAsH pair of peptide chelators,[8] the SNAP/CLIP tags based on engineered DNA alkyltransferase,[9,10] the TMP-tag which exploits the trimethoprim inhibition of *E. coli* dihydrofolate reductase (eDHFR),[11] HaloTag which originated from a haloalkane dehalogenase,[12] β-lactamase-tag,[13] and photoactive yellow protein-based systems.[14,15] To date, HaloTag and SNAP-tag represent the most popular tools in this category. The excellent biochemical specificity of these tags, plus their simple protocol and commercial availability, have enabled a variety of applications ranging from protein manipulation,[16,17] and degradation,[18,19] to metabolite sensing.[20] Notably, self-labeling tags are changing the routine of live-cell imaging in this decade. Rivaling fluorescent proteins, synthetic fluorophores that offer brighter and longer-lasting optical signals in more parallel channels, particularly in far-red and near-IR, can now be easily employed in protein-specific imaging applications.[21] Consequently, self-labeling tags have been increasingly recognized as a future solution in nanoscopy, single-molecule biophysics, and live-cell physiology.[22–24] In the coming era of multiplexed live-cell analysis and imaging at unprecedented spatial-temporal resolutions, both the imaging field and the biological-science field demand a constantly expanding and evolving palette of self-labeling tags. Therefore, delivering a handful of ideal self-labeling tags that are small and non-interruptive, fast-labeling yet specific, and compatible with good fluorophores while remaining mutually orthogonal, has become a challenge for the field of chemical biology.

[*] J. Mo,[+] J. Chen,[+] Y. Shi, Y. Wu, J. Zhang, Z. Chen
National Biomedical Imaging Center, Beijing Key Laboratory of Cardiometabolic Molecular Medicine, College of Future Technology, Peking University
Yiheyuan Road No.5, Beijing 100871 (China)
E-mail: zhixingchen@pku.edu.cn

J. Sun, Z. Chen
PKU-Nanjing Institute of Translational Medicine
Nanjing 211800, Jiangsu (China)

T. Liu, Y. Zheng, Y. Li, Z. Chen
Peking-Tsinghua Center for Life Science
Peking University, Beijing
Yiheyuan Road No.5, Beijing 100871 (China)

Y. Zheng, Y. Li
State Key Laboratory of Membrane Biology, PKU-IDG/McGovern Institute for Brain Research, School of Life Science, Peking University
Yiheyuan Road No.5, Beijing 100871 (China)

Y. Li
Chinese Institute for Brain Research
Beijing 102206 (China)

[+] These authors contributed equally to this work.

Among the existing self-labeling tags, TMP-tag is an appealing technology. Conceptually, in contrast to the suicide substrate-derived SNAP-tag and HaloTag, the development of the TMP-tag and the engineering of its covalent versions were inspired by pharmaceutical chemistry every step of the way. Trimethoprim, the classical antibacterial drug, is a nanomolar binder of eDHFR but does not interfere with mammalian DHFR. Therefore, its structure–activity relationship, selectivity, and *in vivo* behavior have been thoroughly studied.[25] Stemming from the 2005 seminal work,[11] the Cornish lab and others have been continuously developing the eDHFR-TMP system for fluorescence imaging by demonstrating two generations of covalent versions,[26,27] fluorogenic versions,[28,29] and fluorescence-shifting version[30] of TMP-tag. Most of these designs harness the acrylamide-cysteine Michael addition, which is sufficiently reactive to form an adduct near the pocket, but mild enough to avoid non-specific labeling.[26,27,29,30] As a protein tag, the 18 kD monomeric eDHFR consists of only 159 amino acids, making it one of the smallest protein domains among all common self-labeling tags. eDHFR is a thoroughly studied enzyme and tool for biotechnology that has been exploited in numerous applications such as protein degradation[18] and antibody affinity modulation.[31] In the field of fluorescence imaging, however, the development and application of TMP-tag have lagged behind the contemporaneous SNAP-tag and HaloTag, despite a few early employments in the single-molecule imaging of spliceosome assembly[32] and imaging focal-adhesion complex.[33] The latest version of the general TMP-tag in 2012, the second-generation covalent TMP-tag (referred to as TMP2, Figure 1a), was mainly demonstrated with the classical fluorescein and a marginally permeable Atto655.[27] In that version, the covalent addition rendered a permanent linkage that is compatible with fixation, advantageous for long-time imaging. In these years, the importance of bioavailability and fluorogenicity of taggable dyes were gradually recognized and underscored by several biocompatible dyes for advanced imaging.[21,34,35] We reasoned that a further optimized fast-labeling and permeable covalent TMP-acrylamide ligand, in conjunction with modern fluorophores, would bring out the best potential of the TMP-eDHFR pair as the smallest self-labeling protein tag. Such development is not only valuable for adding to the arsenal of labeling technology but also creating the possibility of multiplexed cellular imaging with advanced microscopy.

Here we introduce the third-generation covalent TMP-tag, referred to as TMP-tag3, featuring straightforward synthesis, fast labeling kinetics, significant membrane permeability, and compatibility with state-of-the-art fluorogenic rhodamine dyes. We further assessed the performance of TMP-tag3 by comparative studies with HaloTag and SNAP-tag, focusing on their ligand permeability, protein tag invasiveness, and loop-labeling compatibility. The three orthogonal tags collectively offer a multiplexed labeling solution to cellular proteins, as showcased by three-color live-cell confocal and stimulation emission depletion (STED) imaging.

Results and Discussion

We began our new design using the second-generation covalent TMP-tag as a prototype (Figure 1a). The acrylamide electrophile, offering balanced reactivity and specificity, should be inherited, as reaffirmed by both the modern developments of covalent drugs and recent demonstrations of covalent TMP-conjugates.[36] On the protein side, as the α-carbon of L28 is only 7.2 Å away from TMP 4′ oxygen, it was repeatedly selected as the optimal Cys mutation site in both the second-generation design and various fluorogenic strategies for TMP-tag.[27,28,30] Therefore, L28 remained our first choice to deploy the cysteine nucleophile. Having these two motifs pinned down, we optimized the linkers between TMP, acrylamide, and the fluorophore. In the second-generation design, TMP was first functionalized with a three-carbon linker, followed by coupling with the acryloyl aspartic acid, resulting in a 10-bond length between the 4′ oxygen of TMP and the terminal carbon of acrylamide. The model of the eDHFR-TMP three-dimensional structure suggested that the linker could be shortened further. Therefore, we proposed to functionalize TMP with a two-carbon amine and directly acrylate on this nitrogen. The fluorophore could be derived from the same nitrogen as well. On the fluorophore side, as modern spirolactone/lactam rhodamines leverage residuals on protein surfaces to render fluorogenicity,[34,35,37] the linker between dye and adaptor should be kept minimal. The PEG linker in previous designs was recognized as redundant and therefore abandoned. Having considered the synthetic modularity of the molecule for last-step fluorophore conjugation, we planned to place a rigid phenyl ring between the adaptor nitrogen and the amine conjugation site to prevent intramolecular Michael addition. The new design featured a compact arrangement between TMP, acrylamide, and the fluorophore, with only a 6-bond length between the 4′ oxygen of TMP and the terminal carbon of acrylamide. Based on the new ligand and eDHFR:L28C, a model was built using Maestro (version 12.0, Schrödinger). We confirmed that the acrylamide was within reach of the proximal thiol (Figure 1c), promising faster conjugation kinetics compared to the second-generation design.

The synthetic route toward new TMP-tag derivatives is summarized in Figure 1b. TMP-phenol (**1**), prepared by HBr deprotection from commercially available trimethoprim, was alkylated with a two-carbon extender to give **2**, whose amino group was subsequently released in acid to yield amine **3**. This key amine was first converted to an imine and then reduced with mild $NaBH_3CN$ to yield secondary amine **4**. The acrylamide electrophile was introduced by a condensation reaction with acrylic acid, using 4-(4,6-dimethoxy-1,3,5-triazine-2-yl)-4-methylmorpholinium chloride (DMTMM) as the coupling reagent.[38] The secondary amide is presented as a pair of conformational isomers under proton NMR, which cannot be separated using chromatographical methods. After deprotection with HCl, the universal precursor of the third generation covalent TMP-tag conjugates, **TMP3-NH_2**, was obtained. This route features a straightforward assembly in six chemical steps, which is simpler than previous designs

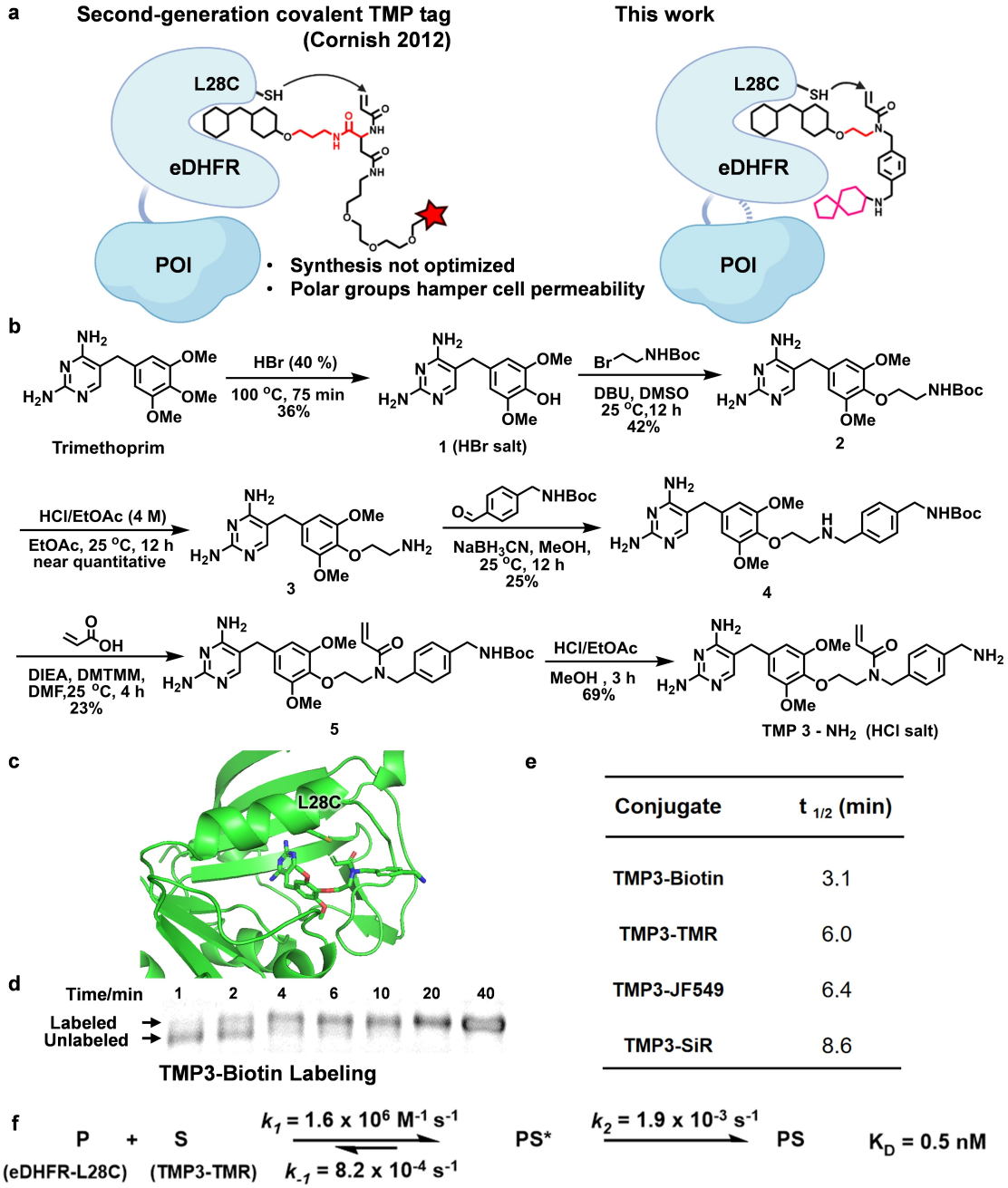

Figure 1. Third-generation covalent TMP-tag enables a fast proximity-induced Michael addition between eDHFR:L28C-fused protein and TMP-acrylamide-conjugates. a) TMP-tag was further optimized in this work toward a closer electrophile-L28C distance, with a minimal linker to the fluorophore, and was assessed for protein loop labeling. b) Synthetic route of third-generation TMP-acrylamide-amine, the precursor for TMP3-labels. c) A structural model showing that the new linker was sufficient for rendering fast proximal-induced reactivity. d) *In vitro* gel-shift assay showing a 3-min half-life of the covalent addition between 10 μM TMP3-Biotin and 5 μM eDHFR:L28C in the presence of 50 μM NADPH at 37 °C. e) TMP3-dyes generally label eDHFR:L28C in a covalent manner with a half-life of <10 min. f) The experimentally determined labeling kinetics of TMP3-TMR in presence of NADPH. P: protein eDHFR-L28C, S: TMP3-TMR, PS*: protein substrate complex, and PS: protein substrate conjugate.

while closely positioning the acrylamide to trimethoprim. A series of TMP3 derivatives were readily prepared through a final-step amide bond formation, including TMP3-Biotin, TMP3-JF549,[39] TMP3-tetramethylrhodamine (TMR), TMP3-SiR,[34] and TMP3-MaP555.[35]

Next, *in vitro* covalent addition was tested using TMP3 conjugates with purified eDHFR. The Cys was introduced at L28, as this variant has been repeatedly proven to be the most reactive nucleophile in TMP-based proximity-induced reactions.[27,28,30] The addition of TMP3-Biotin to eDHFR:L28C produced a gel shift on denaturing SDS-PAGE, which was used to characterize the labeling kinetics. In the presence of 50 μM NADPH, which mimics the cellular environment and tightens the binding of TMP conjugates to

eDHFR,[40] covalent labeling took place at a half-life of 3 min and reached completion in 20 min (Figure 1d and Figure S1). Compared with a half-life of 8 min when using the second-generation covalent TMP-tag, the new design offers >2X faster kinetics with simpler chemistry. Commonly used rhodamines (TMR, JF549, and SiR) could be effectively labeled to eDHFR:L28C using TMP3. An in-gel fluorescence saturation assay indicated that the covalent conjugation of TMP3-rhodamines generally had half-lives of less than 10 min (Figure 1e and Figure S1). These *in vitro* assays established TMP3 as a viable strategy to covalently label molecules to eDHFR:L28C with fast kinetics.

To fully characterize the labeling reaction kinetics of TMP3-dyes using a multi-step kinetic model (Figure 1f), we conducted a biolayer interferometry assay and analyzed the association and dissociation curves (Figure S2). We used the same dye (TMR) to compare the labeling kinetics of TMP3 to the previously reported dynamics of HaloTag and SNAP-tag[41] (Figure 1f, Table S1). In the presence of NADPH, the k_1 of TMP3-TMR to eDHFR is $1.6\times10^6\ M^{-1}s^{-1}$, a comparable number to that of Halo-TMR, confirming the instantaneous non-covalent interaction. TMP3 has the smallest k_{-1} of $8.2\times10^{-4}\ s^{-1}$, giving rise to an apparent 0.5 nM affinity with eDHFR:L28C, which is much smaller than that of Halo and SNAP. As $k_1 \gg k_{-1}$ and *in vitro* labeling reactions were carried out at protein concentrations (5 μM) far higher than the K_D, the in-gel fluorescence saturation assay essentially measured the irreversible covalent addition rate k_2 to be $1.9\times10^{-3}\ s^{-1}$, the slowest among the compared tags. For comparison, the apparent second-order reaction rate constant of TMP3-TMR, k_{app}, was calculated to be $1.1\times10^6\ M^{-1}s^{-1}$ using the equation $k_{app}=k_1k_2/(k_2+k_{-1})$ (Table S1). This number, however, is but a suggestive parameter in assessing the labeling between different tags as the nM level non-covalent binding of TMP3 to eDHFR with NADPH in cells would practically consume a considerable amount of free ligands, deviating the kinetic model from an apparent second-order as in the HaloTag and SNAP-tag.[41] Overall, the non-covalent ternary complex would form completely within 10 min,[42] followed by covalent attachment completed in ≈30 min. This time scale is compatible with practical cell labeling protocols, especially given that the kinetics bottleneck is usually the permeability of ligands.[35] With the newly devised rapid covalent addition, the third-generation TMP-tag rendered additional irreversibility for the fast labeling of proteins in live cells.

Having confirmed rapid covalent labeling of TMP3 dyes to eDHFR:L28C, the pair was tested for live-cell imaging experiments. In the past decade, a handful of fluorogenic rhodamines were developed based on the judiciously tuned spirolactone/zwitterion equilibrium.[34,35,37] These dyes, most commonly demonstrated with HaloTag and SNAP-tag, bear superior membrane permeability and reduced background fluorescence. SiR and MaP555, two representative dyes in the far-red and red channels, were conjugated to TMP3 (Figure 2a). We also synthesized TMP2-SiR for a comparison. While TMP3 conjugates exhibited >10 X fluorescence turn-on behaviors upon the addition of eDHFR:L28C (Figure 2b), TMP2-SiR showed strong baseline fluorescence and marginal (1.2X) turn-on ratio with eDHFR:L28C (Figure S3). Therefore, the linker between TMP and SiR plays important role in manipulating the equilibrium of SiR.

For cellular protein targets, five proteins that localized in different organelles were selected: histone H2B located in nuclei; Sec 61b, an endoplasmic reticulum complex that translocates proteins; MAP7, a microtubule-associated protein; Lifeact, a 17-amino-acid peptide marker that recognizes filamentous actin[43] and Tomm20, a subunit of the translocase of the outer mitochondrial membrane complex. eDHFR:L28C was genetically fused to the N or C termini of these proteins/peptides. All the constructs gave expected labeling patterns at their designated organelles (Figure 2c,d) in live HeLa cells. The superior optical properties of fluorogenic rhodamines further enabled live-cell STED imaging using TMP3. Lifeact-eDHFR:L28C stained with TMP3-SiR gave the fine structure of actin filaments, while Tomm20-eDHFR:L28C stained with TMP3-SiR exhibited the characteristic hollow structure of mitochondrial outer membranes. These fine features were at the boundary of the diffraction limit and were therefore hard to resolve under confocal microscopy (Figure S4). Live-cell imaging results confirmed that eDHFR is a general protein tag for mammalian cytosolic proteins and, at the same time, established the compatibility of TMP3 with fluorogenic SiR and MaP555 for nanoscopy.

In the field of self-labeling protein tags, HaloTag and SNAP-tag have been widely available for practical uses. To profile the relative advantages and weaknesses of different tags, we then systematically performed comparative studies of TMP3, HaloTag, and SNAP-tag.

First, we assessed the cell permeability of their ligands, a recently recognized key parameter in labeling cellular protein targets.[35] The SiR conjugates of CA-NH_2 the Halo ligand, BG-NH_2 the SNAP ligand, and TMP3-NH_2 were prepared and purified using reverse-phase HPLC. According to their ClogP (predicted by ChemDraw), CA-SiR (7.27) was the most lipophilic, TMP3-SiR (7.15) and BG-SiR (7.05) were relatively less lipophilic, while TMP2-SiR (5.33) was the most hydrophilic. We first explored the difference between TMP2 and TMP3 in cell permeability by confocal microscopy. HeLa cells transiently expressing 2X NLS-Halo-eDHFR:L28C-SNAP-GFP were stained with 500 nM TMP2/TMP3-SiR conjugates. Owing to the fluorogenicity of the SiR dye, the staining-imaging process was compatible with a wash-free protocol and was therefore monitored at different time points by a confocal microscope (Figure S5). More than 15 cells were analyzed at each time point, and the staining intensity was plotted (Figure S6). TMP2-SiR showed much slower staining kinetics than TMP3-SiR in live cells. As TMP2-SiR is more hydrophilic, it took almost 2 h to enter cells and nucleus. We attribute this slow cell entry to the polar groups in the linkers of TMP2. In addition, the saturated brightness of TMP2-SiR in the nucleus is only about 60 % of that of TMP3-SiR. Overall, TMP3 is far superior to TMP2 in living cell labeling and imaging. We then performed similar comparative studies of TMP3, HaloTag, and SNAP-tag by a high-content imager using time-lapse mode. More than 200 cells were analyzed in a

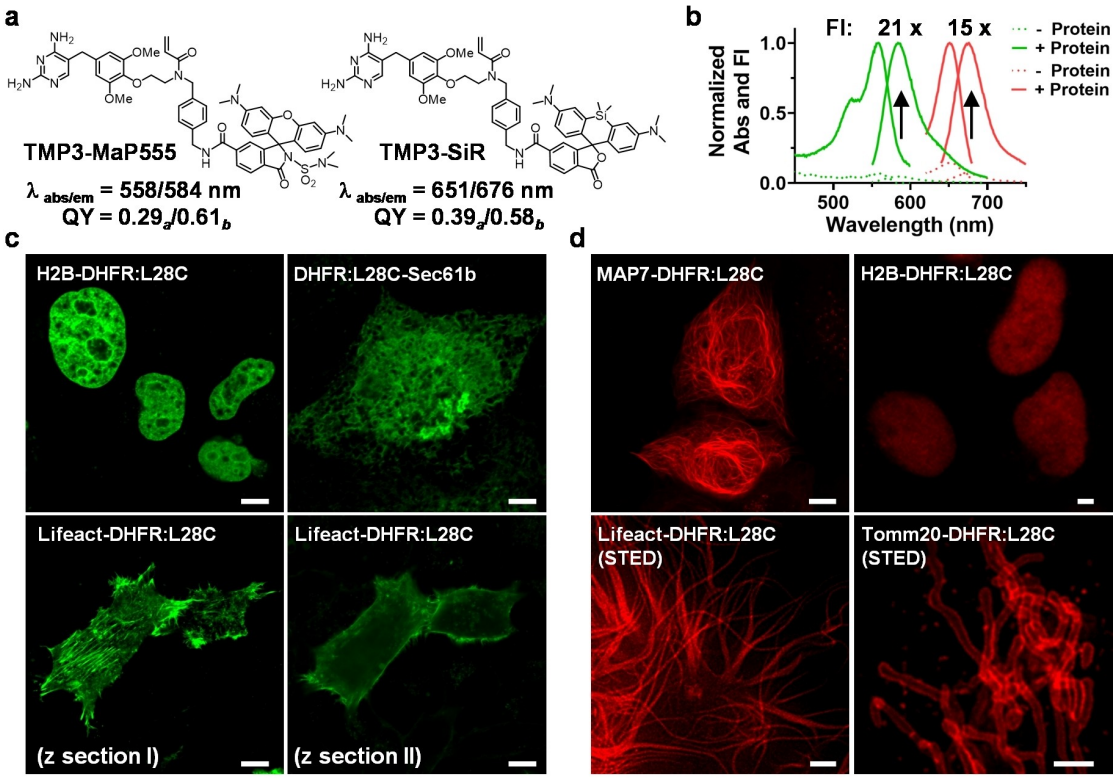

Figure 2. Third-generation covalent TMP-tag in live-cell protein-specific imaging. a) Chemical structures and photophysical properties of TMP3-MaP555 and TMP3-SiR. QY- quantum yield, *a*: binding with eDHFR:L28C in PBS (pH 7.4), *b*: 0.1% SDS in PBS buffer (pH 7.4). b) Absorption and fluorescence spectra of TMP3-MaP555 and TMP3-SiR (10 μM) before and after the addition of eDHFR:L28C (20 μM) in presence of NADPH (50 μM). c) Confocal images of nucleus-localized H2B, ER-localized Sec61b, and F-actin in HeLa cells. Transiently expressed eDHFR:L28C fusion proteins were visualized with TMP3-MaP555 (500 nM staining for 1 h). Scale bars: 10 μm. d) Confocal and STED images of nucleus-localized H2B, microtubule-associated MAP7, F-actin, and outer mitochondria membrane-localized Tomm20 in HeLa cells. Transiently expressed eDHFR:L28C fusion proteins were visualized with TMP3-SiR (500 nM staining for 1 h). Scale bars: 10 μm for confocal images, 1 μm for STED images.

single run, and the staining intensity was plotted. The relative SiR fluorescence to sfGFP at each time point was fitted to a one-step association model to calculate the cell-entry kinetics. The CA-SiR signal reached saturation in <3 min, whose accurate kinetics was too fast to catch using this assay. TMP3-SiR took $\approx$10 min to reach half-saturation and plateaued after 50 min. BG-SiR, however, exhibited the lowest permeability with a half-saturation time of $\approx$1 h (Figure 3a,b). Scrambling the orders of the protein tags or expressing the tandem proteins in cytosol instead of nucleus only marginally affected labeling kinetics (Figure S7, S8, Table S2). The saturation brightness of the three labels indicated that TMP3-SiR was as bright as CA-SiR, while SiR labeled to SNAP exhibited reduced brightness. Our data corroborated a previous comparative study between HaloTag and SNAP-tag.[44] We then compared the three tags with MaP555-ligands. CA-MaP555 still exhibited the fastest cell entry, while TMP3-MaP555 took 10–40 min to reach half-saturation of the tested cellular targets, and BG-MaP555 took more than 1 h to label half of the same proteins (Figure 3c,d, S7, S8, Table S2). Interestingly, the saturated brightness of MaP555 labeled with TMP3 was much lower than the HaloTag counterpart and slightly lower than that of the SNAP-tag. This may be attributed to an incomplete opening of spirolactam at the DHFR surface, which in principle could be further optimized with a fine-tuned spirolactam library.[45]

Based on these results, the lipophilic chloroalkyl ligand of HaloTag rendered fluorophore with a superior cell-permeability, while TMP3-SiR and TMP3-MaP555 were also practically permeable. Our recommendation rank is HaloTag > TMP-tag3 > BG ligands of SNAP-tag for cellular protein labeling applications where labeling speed is important.

Second, we evaluated the compatibility of the protein tags by fusing the three tags with selected protein subunits of mitochondrial machinery. ATP synthase membrane subunit E (ATP5ME) and Cytochrome C oxidase subunit 8A (COX8A), two characteristic subunits in the crowded mitochondrial inner membrane, were selected for tag fusion tests. Mitochondria targeting sequence (MTS)-fused tags were constructed as positive controls. For comparison, the tags were directly fused to the C-termini without flexible linkers. The localizations of the fusion proteins were examined after staining with their corresponding ligand-SiR conjugates. eDHFR:L28C and SNAP-tag fused proteins gave clean mitochondrial patterns. However, without judiciously optimized linkers between protein and tags,

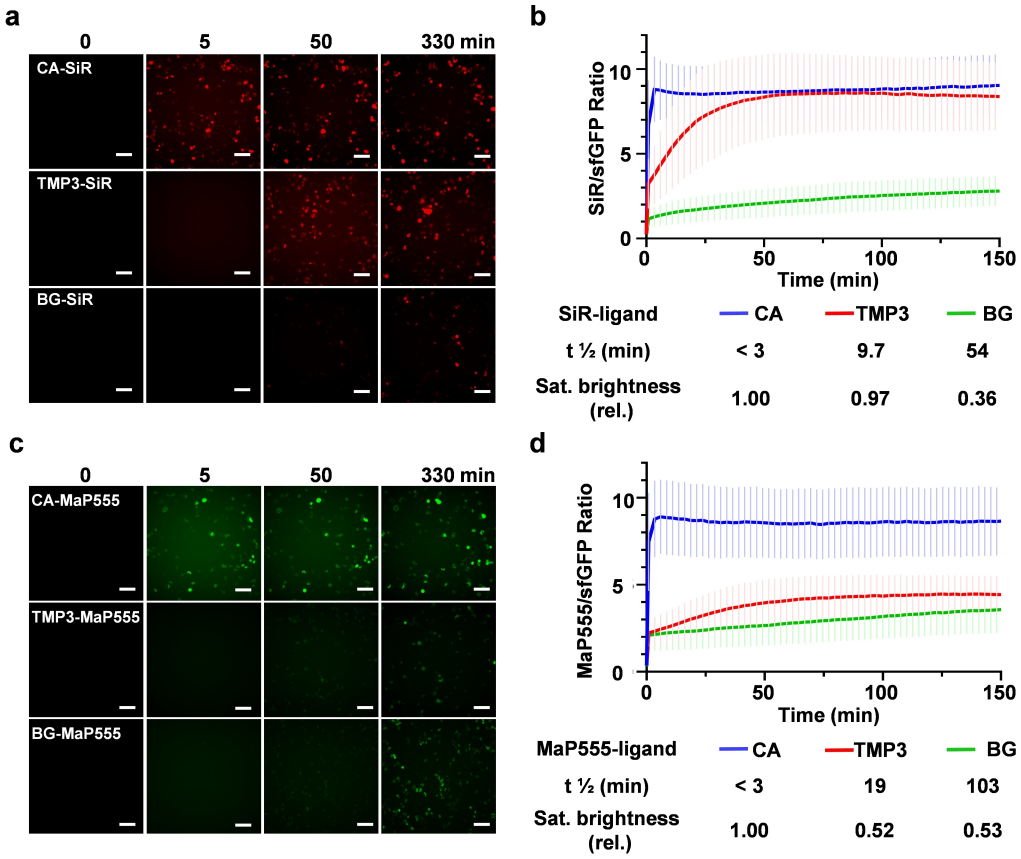

Figure 3. TMP3-SiR and TMP3-MaP555 were practically permeable dyes for live-cell protein labeling. a) COS-7 cells transiently expressing 2X NLS-SNAP-eDHFR:L28C-Halo-GFP stained with 500 nM SiR ligands. The staining processes were continuously monitored and analyzed using a high-content imager under epi-fluorescence mode to produce intensity curves over time. b) Relative intensity plot of the staining process reveals the cell-entry half-life and the saturation brightness of each SiR-ligand. c) COS-7 cells transiently expressing 2X NLS-SNAP-eDHFR:L28C-Halo-GFP stained with 500 nM MaP555 ligands. The staining processes were continuously monitored and analyzed using a high-content imager under epi-fluorescence mode to produce intensity curves over time. d) Relative intensity plot of the staining process reveals the cell-entry half-life and the saturation brightness of each MaP555-ligand. Scale bars: 100 μm.

ATP5ME-Halo and COX8A-Halo mislocalized into the endoplasmic reticulum or cytosol (Figure 4). The addition of a 5aa linker (GGGGS) between COX8A and Halo did not remedy the mitochondrial localization, giving a similar non-mitochondrial distribution (Figure S9). We tentatively attributed the observed mislocalization of mitochondrial protein fusions to the relatively larger size of HaloTag (36 kD) compared to the smaller eDHFR (18 kD) and SNAP-tag (19 kD), which may affect the assembly of certain subunits of protein machineries. A recent successful demonstration of HaloTag fused to COX8A exploited four tandem repeats of truncated COX8 A flanked by a human sepiapterin reductase to realize mitochondrial localization[46] (addgene #113916, see Supporting Information for sequence). This evidence corroborated the fact that small protein tags are advantageous in fusing proteins that are spatially demanding.

Overall, while protein fusions are largely based on try-and-error approaches, the TMP-DHFR pair, bearing a reasonable permeability and a compact size, provides promising options besides HaloTag and SNAP-tag for fast labeling proteins that are sensitive to fusion tags, such as those located in congested environments.

Besides the classical way of fusing tags at the N/C terminal of target proteins, modern protein architectural engineering has increasingly focused on protein loops.[47] Such initiatives are not only valuable for labeling proteins whose termini are buried or functional,[48] but they also open up larger biochemical spaces for advanced functions such as antibody-drug conjugates[49] and biomaterials.[50] As loop-fusion may affect the structural integrity of both the protein-of-interest and the tag, it represents a rigorous test for the folding and stability of tags (Figure 5a). eDHFR has two advantages as a promising loop tag: 1) The N–C distance of eDHFR is 14.2 Å, while HaloTag and SNAP-tag have N–C distances of 32.5 Å and 39.6 Å, respectively (Figure 5b). 2) As a well-studied model protein for bioengineering, eDHFR has been inserted into proteins ranging from YFP[51] to nanobodies[31] for functional-regulation purposes. We, therefore, tested loop fusion and labeling using TMP-tag3 on various proteins of interest to explore this potential.

First, we attempted to insert eDHFR into firefly luciferase at different loops. A number of breaking points at

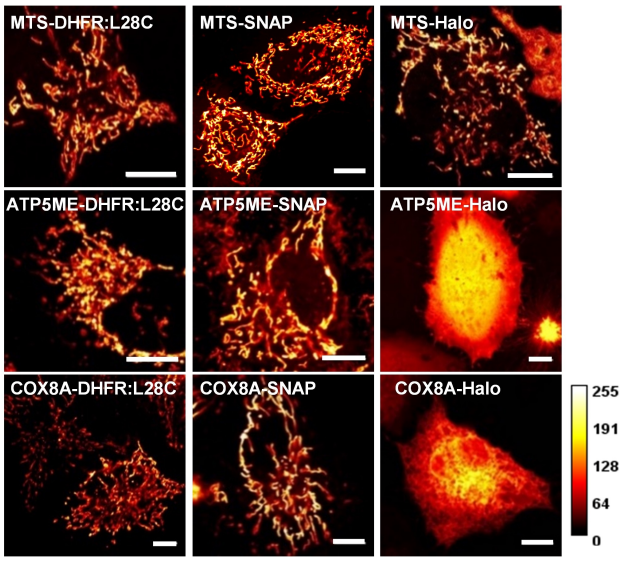

Figure 4. Localization of selected mitochondrial proteins fused with eDHFR:L28C, SNAP, or Halo in HeLa cells. Cells are stained with corresponding SiR ligands before imaging by a confocal microscope. HaloTag exhibited cytosolic mislocation when fused directly to selected mitochondrial proteins. MTS: mitochondria targeting sequence; ATP5ME: ATP Synthase Membrane Subunit E, located on the inner membrane of mitochondria; COX8A: Cytochrome C Oxidase Subunit 8 A, located on the inner membrane of mitochondria. Scale bars: 10 μm.

different loops were screened: T74/N75, Y178/D179, F331/H332, V384/N385, R437/L438, S504/Q505, and T508/A509 (Figure 5c). The N and C termini of eDHFR were inserted along with three flexible amino acids (GGS and GSG) as linkers (see Supporting Information for the full sequences). Assayed in *E. coli* lysates, luciferase activities were compromised in all the loop fusion constructs, but not in the terminal-fusion counterparts (Figure 5d). Among the loop-fusion positions, T508/A509 fusion, marked as Luc-508-DHFR, exhibited the highest luminescence. At this position, the loop tag was then substituted with eDHFR:L28C, HaloTag, and SNAP-tag. For the Halo and SNAP fusions, a pair of 10-aa linkers were added. All three loop-inserted tags can be labeled with TMR conjugates, indicating a comparable expression level (Figure S10). Although the pair of 10-aa linkers were sufficient to connect the gaps between the N/C termini of all tags in principle, eDHFR:L28C insertion at the 508 position exhibited a higher luminescence activity than the Halo and SNAP counterparts (Figure 5e), representing a least-interruptive loop tag for firefly luciferase.

Second, we compared the insertion of eDHFR:L28C, HaloTag, and SNAP-tag into superfolder GFP (sfGFP), a stabilized version of the enhanced GFP featuring a robust folding.[52] The loop between strands 10 and 11 was selected as the inserting point, as suggested by the routine practice of split GFP.[53] Two 10-aa linkers were inserted between sfGFP and eDHFR (Figure 5f). The constructs were expressed under the T7 promoter in *E. coli.* After induction, the strains expressing sfGFP1-10-(eDHFR:L28C)-sfGFP11 were ≈50 % fluorescent as that of WT sfGFP, while the SNAP- and Halo- inserted sfGFP only exhibited <10 % fluorescence compared to WT sfGFP (Figure 5g). These loop-tagged sfGFPs were purified, and their absolute fluorescent quantum yields were measured using a steady-state spectrometer. All the variants had a similar quantum yield near 75 %, similar to WT sfGFP, indicating an intact core structure of the chromophore (Table S3). Therefore, the fluorescence difference of the three loop-tags was mainly attributed to expression levels, as further confirmed by gel densitometry analysis (Figure 5h). The loop-inserting eDHFR:L28C at sfGFP could be labeled with TMP3-TMR, as confirmed by FRET characterization with its fluorescence emission spectrum (Figure S11). Overall, the insertion of eDHFR, SNAP, and Halo at the loop between strands 10 and 11 of sfGFP did not affect fluorescence, but the eDHFR fusion rendered an outstanding expression level.

Our third attempt was the construction of an eDHFR fusing on the loop of another eDHFR to explore the labeling kinetics of TMP3 to both the inserted and inserting protein tags. The insertion site was selected at N23/L24, as this loop was exploited before for circular permutation of eDHFR.[31,54] L28C mutations were introduced to both the inserting eDHFR and the inserted eDHFR (Figure 5i). Labeling kinetics were calculated from fluorescence densitometry of an *in vitro* labeling assay. The half-life of TMP3-TMR labeling the inserting eDHFR:L28C was 12 min, close to that of the monomeric eDHFR:L28C (6 min). Labeling of the inserted eDHFR:L28C, however, exhibited a decreased reactivity (half-life of 49 min, Figure 5j) which could be attributed to the proximity of L28C to the insertion site at N23/L24. Overall, this result showcased the structural integrity of eDHFR as both a loop tag and a functional protein.

Finally, we examined the loop-fusion of eDHFR:L28C into a membrane protein: Human Dopamine Receptor D1 (DRD1). As a G-protein-coupled receptor, the third intracellular loop (ICL3) is often selected for protein engineering.[55,56] After insertion of eDHFR:L28C into the ICL3 of DRD1 (Figure 5k), the fusion gene was transiently expressed in HeLa cells, and TMP3-SiR staining gave a distinctive membrane localization that colocalized with a plasma-membrane-localized GFP marker (Figure 5l).

While loop-fusion tags are still in their infancy and often demand additional screening and optimization compared to classical terminal fusions, these results establish TMP-tag3 as a viable option for labeling the loops of cytosolic and membrane proteins. Echoing the emerging examples using circular-permutated self-labeling protein tags, these architecturally sophisticated protein chimeras represent the fundamental elements for future biomaterials and hybrid sensors.[57,58]

TMP-tag3, HaloTag, and SNAP-tag are not only complementing approaches, their orthogonality enables the combinatory use for multiplexed labeling and imaging. We first showcased simultaneous imaging of Tomm20 and F-actin. HeLa cells transiently expressing Lifeact-eDHFR:L28C and Tomm20-Halo were stained with TMP3-SiR and Halo-TMR. Confocal imaging gave filament and outer

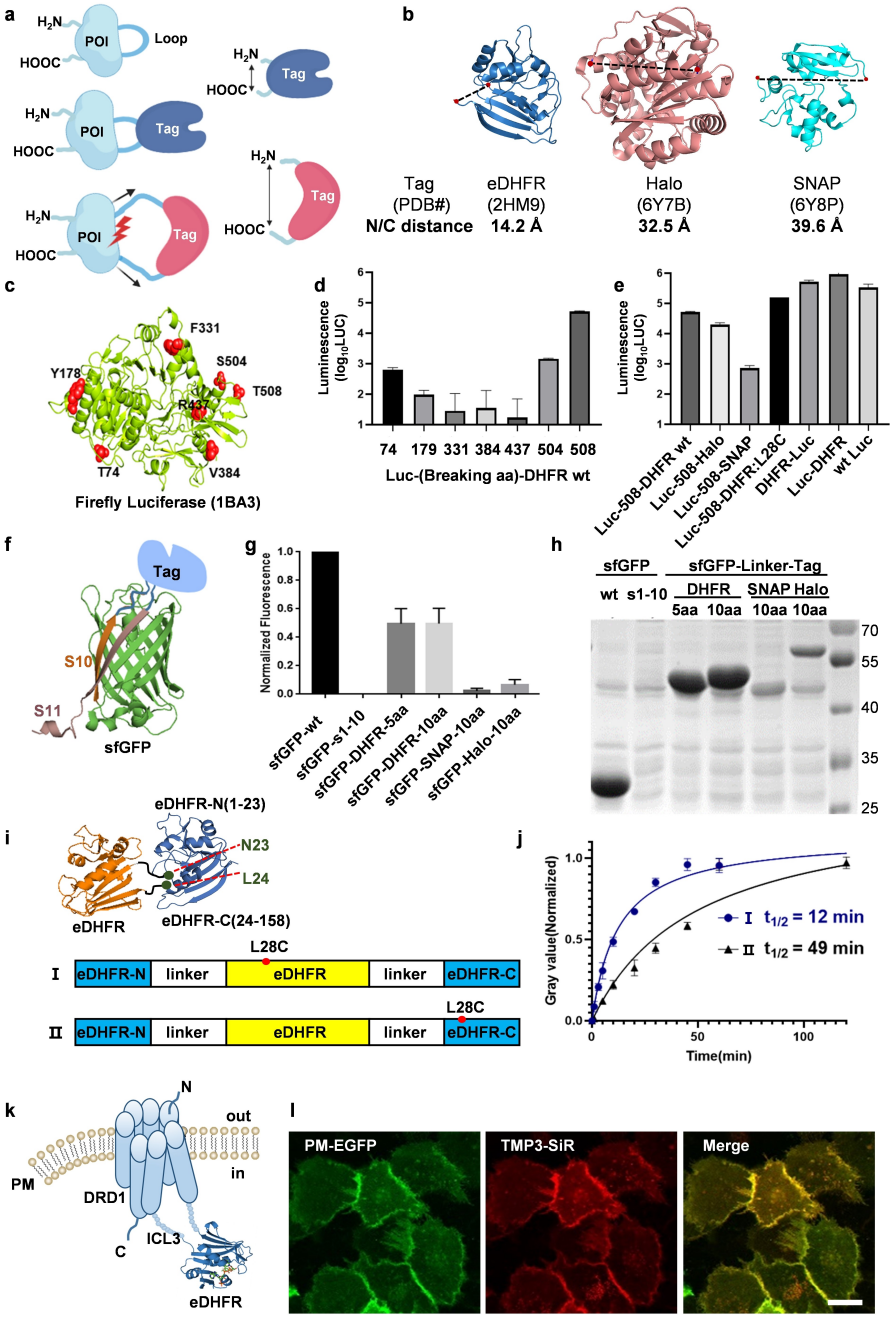

Figure 5. TMP3-eDHFR was superior for labeling the loops of proteins. a) Schematic illustration of protein loop fusion and the challenge posed for protein tags. b) The N–C terminal distance of eDHFR was 1.4 nm, much shorter than those of Halo (3.3 nm) or SNAP (4.0 nm). c) eDHFR was inserted into firefly luciferase at the selected loop sites. d) Among the eDHFR insertions, the S508 site exhibited the least reduction in luminescence. e) Comparison of luminescence between eDHFR, Halo, and SNAP-inserted Fluc, along with wt Fluc and Fluc-eDHFR terminal fusions. f) Schematic illustration of the loop between sfGFP S10 and S11 inserted with eDHFR, Halo, and SNAP. g) Fluorescence of *E. coli* expressing WT, S1-10 truncated, and loop-fused sfGFP. h) SDS-PAGE analysis of *E. coli* lysate showing the expression level of WT, S1-10 truncated, and loop-fused sfGFP. i) Schematic illustration of an eDHFR inserted into another eDHFR at the N23/L24 site. The two eDHFRs were introduced with L28C mutations. j) In-gel fluorescence densitometry assay showing the labeling kinetics on the inserted and inserting eDHFR:L28C. k) Schematic illustration of an eDHFR inserted into the third intracellular loop of dopamine receptor D1 (DRD1), a membrane protein of the GPCR family. l) Live-cell confocal images of DRD1-eDHFR:L28C loop fusion labeled with TMP3-SiR, and the colocalization with a membrane-anchored EGFP marker.

mitochondrial membrane patterns. The fine patterns of actin and mitochondria were unambiguously resolved in the two channels (Figure 6a). It is noteworthy that the minor displacement of the mitochondrial patterns between the confocal and STED images was attributed to cellular movement within the experimental interval (≈10 sec) during the

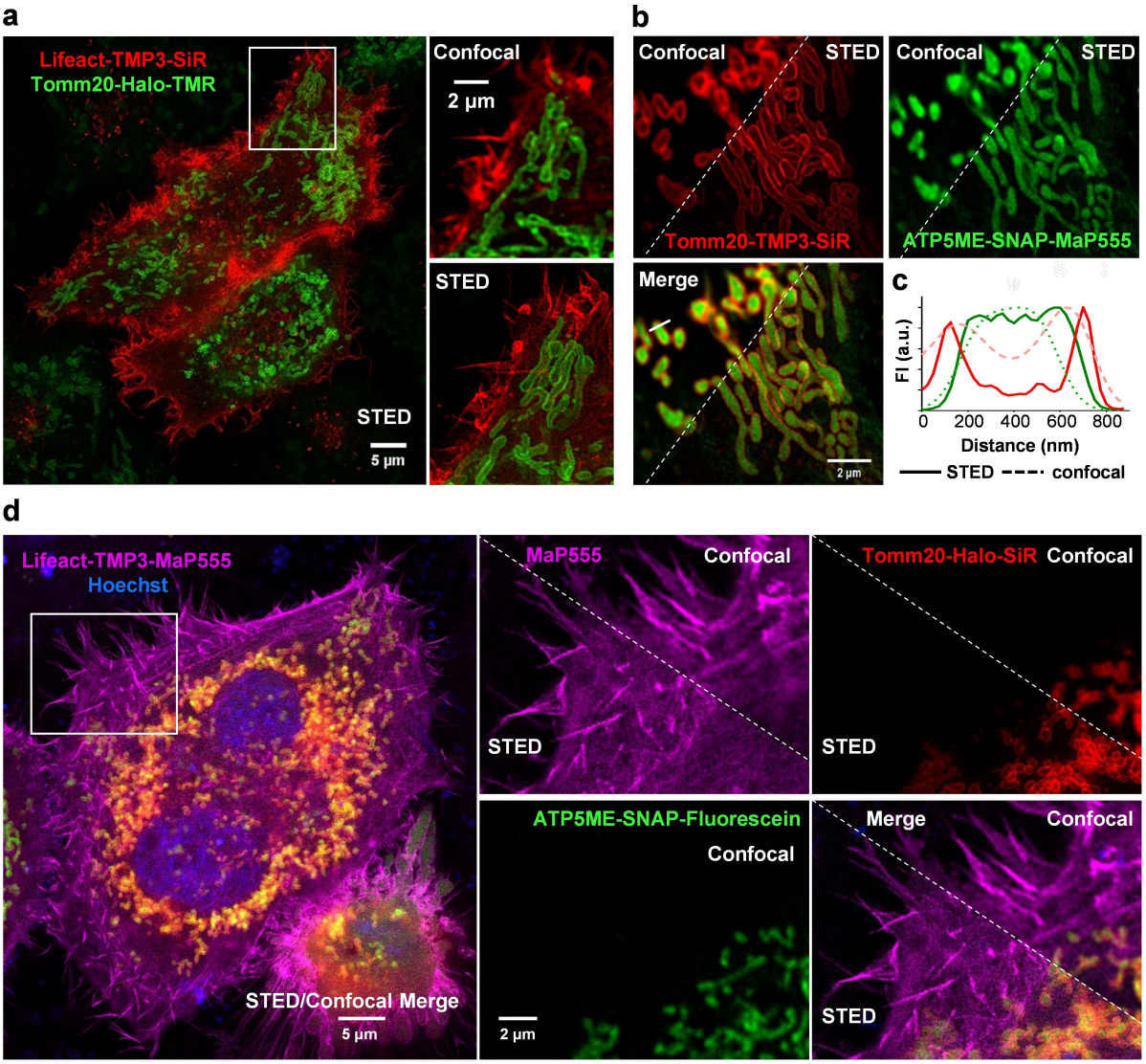

Figure 6. TMP-tag3, HaloTag, and SNAP-tag enabled orthogonal protein labeling for multi-color STED imaging in live HeLa cells. a) Two-color confocal and STED images of mitochondria outer-membrane and F-actin. HeLa cells transiently expressing Lifeact-eDHFR:L28C and Tomm20-Halo were stained with 250 nM TMP3-SiR and 250 nM Halo-TMR for 1 h before imaging. b) Two-color confocal and STED images of Tomm20 and ATP synthase membrane subunit E. HeLa cells transiently expressing Tomm20-eDHFR:L28C and ATP5ME-SNAP were stained with 200 nM TMP3-SiR and 400 nM SNAP-MaP555 for 1 h before imaging. c) Intensity profile plot along the white line shown in the merge channel. The outer membrane of a selected mitochondrion was resolved in the STED image. d) Four-color confocal and STED images of actin, Tomm20, ATP synthase membrane subunit E, and nucleus. HeLa cells transiently expressing Lifeact-eDHFR:L28C, Tomm20-Halo, and ATP5ME-SNAP were stained with Hoechst, 250 nM TMP3-MaP555, 250 nM CA-SiR, and 500 nM BG-fluorescein for 1.5 h before imaging.

imaging-mode switch. We then tested two-color mitochondrial labeling using the two smaller tags: TMP3 and SNAP. Tomm20-eDHFR:L28C was labeled with TMP3-SiR, and ATP5ME-SNAP was labeled with SNAP-MaP555. After 400 nM dye staining for 1 h, Tomm20 gave a distinctive outer mitochondrial membrane pattern under STED nanoscopy, while ATP5ME was located in the inner membrane and matrix (Figure 6b). Intensity profiles were plotted across a mitochondrion to compare the resolution of the STED and confocal images (Figure 6c). In the STED channels, the outer-membrane-localized Tomm20 and inner-membrane-localized ATP synthase membrane subunit E were resolved.

Finally, HeLa cells transiently expressing three tagged proteins were labeled and imaged with three dye conjugates. In this setup, TMP3-MaP555 was labeled to F-actin via Lifeact-eDHFR:L28C, CA-SiR stained Tomm20, and ATP5ME were labeled with BG-fluorescein. Four-color live-cell images were successfully acquired, among which the TMP3-MaP555 and Halo-SiR channels were compatible with STED nanoscopy (Figure 6d). Fluorescein was not compatible with STED imaging but the confocal channel gave a characteristic mitochondrial pattern. The morphology of the cells in this experiment was compromised partly due to the burden of overexpression of multiple transiently

expressed genes. This issue could be potentially addressed by tuning the expression levels.

Overall, we demonstrated the labeling and imaging of up to three protein targets with orthogonal self-labeling tags. The third-generation covalent TMP tag, along with HaloTag and SNAP-tag, is expected to expand the chemical biology toolkit for multiplexed protein analysis under nanoscopic imaging in the big data era.

Conclusion

Herein, we devised the third generation of the covalent TMP-tag for live-cell protein labeling and performed comparative studies with HaloTag and SNAP-tag. TMP-tag3, featuring optimized linkers and compatibility with fluorogenic rhodamine dyes, can now supplement and supplant the existing HaloTag and SNAP-tag technologies in different aspects. Overall, HaloTag still bears the best labeling speed and bioavailability and is therefore considered the first choice for versatile protein labeling. In cases where the fusion of the 36 kD HaloTag fails to maintain protein function, the 18-kD TMP-tag3 and 19-kD SNAP-tag offer supplemental solutions. TMP-tag3 exhibits satisfactory cell permeability and generally outperforms the BG conjugates of SNAP-tag in labeling cellular targets. On the flip side, the current TMP-tag3 still prefers the addition of an NADPH cofactor, and the covalent addition step is not as fast as that of HaloTag and SNAP-tag, limiting its applications in *in vitro* labeling. This issue, however, is not a fundamental limit and is subject to further optimization of both the ligand and protein. This work adds to the diverse strategies for the evolution of tags,[46] showcasing the links between protein engineering, substrate optimization, and innovations in fluorophores.

The self-labeling tag toolbox, however, should not be seen as a winner-takes-all arena. Rather, with the addition of TMP-tag3, the multiplexed use of tags has more opportunities in the era of nanoscopy, 4D physiology, and big data. Exemplified by the emerging Brainbow,[59] nonlinear Raman spectroscopy,[60] lifetime multiplexing,[46] and CODEX technologies,[61] bioimaging has never been more focused on multiplexing. Orthogonal tags, plus ever-expanding fluorophore palettes with superior optical properties, promise to interrogate multiple organelles and molecular targets into live cells over long stretches of time beyond the traditional diffraction limit. These directions have the potential to revolutionize the routine of cell biology and cell phenotyping.

Acknowledgements

This work was supported by the National Natural Science Foundation of China (Project 31971375 to Z.C.), Beijing Municipal Science & Technology Commission (Project: Z201100005320017 to Z.C.), National Key R&D Program of China (2021YFF0502904 to Z.C.), Peking-Tsinghua Center for Life Sciences (to Z.C. and Y.L.), and a start-up fund from Peking University (to Z. C.). We thank Profs. Chu Wang, Zhen Yang, and Jia-Hua Chen for sharing their chemistry labs, Profs. Heping Cheng and Xianhua Wang for sharing mitochondrial genes and instruments, Prof. Peng Zou, Prof. Lu Wang, Dr. Bei Liu, Yuan Zhang, and Dr. Yongxian Xu for helpful discussions, and Rui Sang and Yong Li for experimental assistance. We thank the Metabolic Mass Spectrometry Platform of IMM, the analytical instrumentation center of Peking University, and the NMR facility and optical imaging facility of the National Center for Protein Sciences at Peking University for assistance with data acquisition.

Conflict of Interest

Z.C., J.M., J.C., and J.S. have submitted a patent application based on the TMP conjugates described in this work.

Data Availability Statement

The data that support the findings of this study are available from the corresponding author upon reasonable request.

Keywords: Covalent Drug · Live-Cell Imaging · Orthogonal Bioconjugation · Protein Loop Engineering · Self-Labeling Tag

[1] E. M. Sletten, C. R. Bertozzi, *Angew. Chem. Int. Ed.* **2009**, *48*, 6974–6998; *Angew. Chem.* **2009**, *121*, 7108–7133.
[2] C. Jing, V. W. Cornish, *Acc. Chem. Res.* **2011**, *44*, 784–792.
[3] T. Peng, H. C. Hang, *J. Am. Chem. Soc.* **2016**, *138*, 14423–14433.
[4] A. Sachdeva, K. Wang, T. Elliott, J. W. Chin, *J. Am. Chem. Soc.* **2014**, *136*, 7785–7788.
[5] C. Uttamapinant, K. A. White, H. Baruah, S. Thompson, M. Fernández-Suárez, S. Puthenveetil, A. Y. Ting, *Proc. Natl. Acad. Sci. USA* **2010**, *107*, 10914.
[6] J. Wang, Y. Liu, Y. Liu, S. Zheng, X. Wang, J. Zhao, F. Yang, G. Zhang, C. Wang, P. R. Chen, *Nature* **2019**, *569*, 509–513.
[7] B. A. Griffin, R. Adams Stephen, Y. Tsien Roger, *Science* **1998**, *281*, 269–272.
[8] S. R. Adams, R. E. Campbell, L. A. Gross, B. R. Martin, G. K. Walkup, Y. Yao, J. Llopis, R. Y. Tsien, *J. Am. Chem. Soc.* **2002**, *124*, 6063–6076.
[9] A. Keppler, S. Gendreizig, T. Gronemeyer, H. Pick, H. Vogel, K. Johnsson, *Nat. Biotechnol.* **2003**, *21*, 86–89.
[10] A. Gautier, A. Juillerat, C. Heinis, I. R. Corrêa, M. Kindermann, F. Beaufils, K. Johnsson, *Chem. Biol.* **2008**, *15*, 128–136.
[11] L. W. Miller, Y. Cai, M. P. Sheetz, V. W. Cornish, *Nat. Methods* **2005**, *2*, 255–257.
[12] G. V. Los, L. P. Encell, M. G. McDougall, D. D. Hartzell, N. Karassina, C. Zimprich, M. G. Wood, R. Learish, R. F. Ohana, M. Urh, D. Simpson, J. Mendez, K. Zimmerman, P. Otto, G. Vidugiris, J. Zhu, A. Darzins, D. H. Klaubert, R. F. Bulleit, K. V. Wood, *ACS Chem. Biol.* **2008**, *3*, 373–382.
[13] S. Mizukami, S. Watanabe, Y. Hori, K. Kikuchi, *J. Am. Chem. Soc.* **2009**, *131*, 5016–5017.
[14] Y. Hori, T. Norinobu, M. Sato, K. Arita, M. Shirakawa, K. Kikuchi, *J. Am. Chem. Soc.* **2013**, *135*, 12360–12365.
[15] M.-A. Plamont, E. Billon-Denis, S. Maurin, C. Gauron, F. M. Pimenta, C. G. Specht, J. Shi, J. Quérard, B. Pan, J. Rossignol,

K. Moncoq, N. Morellet, M. Volovitch, E. Lescop, Y. Chen, A. Triller, S. Vriz, T. Le Saux, L. Jullien, A. Gautier, *Proc. Natl. Acad. Sci. USA* **2016**, *113*, 497.
[16] M. Ishida, H. Watanabe, K. Takigawa, Y. Kurishita, C. Oki, A. Nakamura, I. Hamachi, S. Tsukiji, *J. Am. Chem. Soc.* **2013**, *135*, 12684–12689.
[17] J. Broichhagen, A. Damijonaitis, J. Levitz, K. R. Sokol, P. Leippe, D. Konrad, E. Y. Isacoff, D. Trauner, *ACS Cent. Sci.* **2015**, *1*, 383–393.
[18] Y. Miyamae, L.-c. Chen, Y. Utsugi, H. Farrants, T. J. Wandless, *Cell Chem. Biol.* **2020**, *27*, 1573–1581.
[19] K. Raina, D. J. Noblin, Y. V. Serebrenik, A. Adams, C. Zhao, C. M. Crews, *Nat. Chem. Biol.* **2014**, *10*, 957–962.
[20] Q. Yu, L. Xue, J. Hiblot, R. Griss, S. Fabritz, C. Roux, P.-A. Binz, D. Haas, G. Okun Jürgen, K. Johnsson, *Science* **2018**, *361*, 1122–1126.
[21] J. B. Grimm, L. D. Lavis, *Nat. Methods* **2022**, *19*, 149–158.
[22] Z. Chen, V. W. Cornish, W. Min, *Curr. Opin. Chem. Biol.* **2013**, *17*, 637–643.
[23] J. B. Grimm, B. P. English, H. Choi, A. K. Muthusamy, B. P. Mehl, P. Dong, T. A. Brown, J. Lippincott-Schwartz, Z. Liu, T. Lionnet, L. D. Lavis, *Nat. Methods* **2016**, *13*, 985–988.
[24] L. Wang, M. S. Frei, A. Salim, K. Johnsson, *J. Am. Chem. Soc.* **2019**, *141*, 2770–2781.
[25] D. A. Matthews, J. T. Bolin, J. M. Burridge, D. J. Filman, K. W. Volz, J. Kraut, *J. Biol. Chem.* **1985**, *260*, 392–399.
[26] S. S. Gallagher, J. E. Sable, M. P. Sheetz, V. W. Cornish, *ACS Chem. Biol.* **2009**, *4*, 547–556.
[27] Z. Chen, C. Jing, S. S. Gallagher, M. P. Sheetz, V. W. Cornish, *J. Am. Chem. Soc.* **2012**, *134*, 13692–13699.
[28] C. Jing, V. W. Cornish, *ACS Chem. Biol.* **2013**, *8*, 1704–1712.
[29] W. Liu, F. Li, X. Chen, J. Hou, L. Yi, Y.-W. Wu, *J. Am. Chem. Soc.* **2014**, *136*, 4468–4471.
[30] D. Zhang, R. Liu, C. Bao, C. Zhang, L. Yang, L. Deng, B. Bao, J. Yang, X. Chen, Q. Lin, Y. Yang, L. Zhu, *Bioconjugate Chem.* **2019**, *30*, 184–191.
[31] H. Farrants, M. Tarnawski, T. G. Müller, S. Otsuka, J. Hiblot, B. Koch, M. Kueblbeck, H.-G. Kräusslich, J. Ellenberg, K. Johnsson, *Nat. Methods* **2020**, *17*, 279–282.
[32] A. Hoskins Aaron, J. Friedman Larry, S. Gallagher Sarah, J. Crawford Daniel, G. Anderson Eric, R. Wombacher, N. Ramirez, W. Cornish Virginia, J. Gelles, J. Moore Melissa, *Science* **2011**, *331*, 1289–1295.
[33] X. Hu, C. Jing, X. Xu, N. Nakazawa, V. W. Cornish, F. M. Margadant, M. P. Sheetz, *Nano Lett.* **2016**, *16*, 4062–4068.
[34] G. Lukinavičius, K. Umezawa, N. Olivier, A. Honigmann, G. Yang, T. Plass, V. Mueller, L. Reymond, I. R. Corrêa Jr, Z.-G. Luo, C. Schultz, E. A. Lemke, P. Heppenstall, C. Eggeling, S. Manley, K. Johnsson, *Nat. Chem.* **2013**, *5*, 132–139.
[35] L. Wang, M. Tran, E. D'Este, J. Roberti, B. Koch, L. Xue, K. Johnsson, *Nat. Chem.* **2020**, *12*, 165–172.
[36] A. K. Ghosh, I. Samanta, A. Mondal, W. R. Liu, *ChemMedChem* **2019**, *14*, 889–906.
[37] Q. Zheng, A. X. Ayala, I. Chung, A. V. Weigel, A. Ranjan, N. Falco, J. B. Grimm, A. N. Tkachuk, C. Wu, J. Lippincott-Schwartz, R. H. Singer, L. D. Lavis, *ACS Cent. Sci.* **2019**, *5*, 1602–1613.
[38] M. Kunishima, C. Kawachi, F. Iwasaki, K. Terao, S. Tani, *Tetrahedron Lett.* **1999**, *40*, 5327–5330.
[39] J. B. Grimm, B. P. English, J. Chen, J. P. Slaughter, Z. Zhang, A. Revyakin, R. Patel, J. J. Macklin, D. Normanno, R. H. Singer, T. Lionnet, L. D. Lavis, *Nat. Methods* **2015**, *12*, 244–250.
[40] P. D. Reiss, P. F. Zuurendonk, R. L. Veech, *Anal. Biochem.* **1984**, *140*, 162–171.
[41] J. Wilhelm, S. Kühn, M. Tarnawski, G. Gotthard, J. Tünnermann, T. Tänzer, J. Karpenko, N. Mertes, L. Xue, U. Uhrig, J. Reinstein, J. Hiblot, K. Johnsson, *Biochemistry* **2021**, *60*, 2560–2575.
[42] R. Selvaraj, J. M. Fox, *Curr. Opin. Chem. Biol.* **2013**, *17*, 753–760.
[43] J. Riedl, A. H. Crevenna, K. Kessenbrock, J. H. Yu, D. Neukirchen, M. Bista, F. Bradke, D. Jenne, T. A. Holak, Z. Werb, M. Sixt, R. Wedlich-Soldner, *Nat. Methods* **2008**, *5*, 605–607.
[44] R. S. Erdmann, S. W. Baguley, J. H. Richens, R. F. Wissner, Z. Xi, E. S. Allgeyer, S. Zhong, A. D. Thompson, N. Lowe, R. Butler, J. Bewersdorf, J. E. Rothman, D. St Johnston, A. Schepartz, D. Toomre, *Cell Chem. Biol.* **2019**, *26*, 584–592.
[45] N. Lardon, L. Wang, A. Tschanz, P. Hoess, M. Tran, E. D'Este, J. Ries, K. Johnsson, *J. Am. Chem. Soc.* **2021**, *143*, 14592–14600.
[46] M. S. Frei, M. Tarnawski, M. J. Roberti, B. Koch, J. Hiblot, K. Johnsson, *Nat. Methods* **2022**, *19*, 65–70.
[47] A. H. Keeble, V. K. Yadav, M. P. Ferla, C. C. Bauer, E. Chuntharpursat-Bon, J. Huang, R. S. Bon, M. Howarth, *Cell Chem. Biol.* **2022**, *29*, 339–350.
[48] W.-K. Huh, J. V. Falvo, L. C. Gerke, A. S. Carroll, R. W. Howson, J. S. Weissman, E. K. O'Shea, *Nature* **2003**, *425*, 686–691.
[49] M. Baalmann, L. Neises, S. Bitsch, H. Schneider, L. Deweid, P. Werther, N. Ilkenhans, M. Wolfring, M. J. Ziegler, J. Wilhelm, H. Kolmar, R. Wombacher, *Angew. Chem. Int. Ed.* **2020**, *59*, 12885–12893; *Angew. Chem.* **2020**, *132*, 12985–12993.
[50] P. Bitterwolf, S. Gallus, T. Peschke, E. Mittmann, C. Oelschlaeger, N. Willenbacher, K. S. Rabe, C. M. Niemeyer, *Chem. Sci.* **2019**, *10*, 9752–9757.
[51] R. Rakhit, R. Navarro, Thomas J. Wandless, *Chem. Biol.* **2014**, *21*, 1238–1252.
[52] J.-D. Pédelacq, S. Cabantous, T. Tran, T. C. Terwilliger, G. S. Waldo, *Nat. Biotechnol.* **2006**, *24*, 79–88.
[53] S. Cabantous, T. C. Terwilliger, G. S. Waldo, *Nat. Biotechnol.* **2005**, *23*, 102–107.
[54] T. Nakamura, M. Iwakura, *J. Biol. Chem.* **1999**, *274*, 19041–19047.
[55] D. M. Rosenbaum, S. G. F. Rasmussen, B. K. Kobilka, *Nature* **2009**, *459*, 356–363.
[56] F. Sun, J. Zhou, B. Dai, T. Qian, J. Zeng, X. Li, Y. Zhuo, Y. Zhang, Y. Wang, C. Qian, K. Tan, J. Feng, H. Dong, D. Lin, G. Cui, Y. Li, *Nat. Methods* **2020**, *17*, 1156–1166.
[57] C. Deo, A. S. Abdelfattah, H. K. Bhargava, A. J. Berro, N. Falco, H. Farrants, B. Moeyaert, M. Chupanova, L. D. Lavis, E. R. Schreiter, *Nat. Chem. Biol.* **2021**, *17*, 718–723.
[58] V. Villette, M. Chavarha, I. K. Dimov, J. Bradley, L. Pradhan, B. Mathieu, S. W. Evans, S. Chamberland, D. Shi, R. Yang, B. B. Kim, A. Ayon, A. Jalil, F. St-Pierre, M. J. Schnitzer, G. Bi, K. Toth, J. Ding, S. Dieudonné, M. Z. Lin, *Cell* **2019**, *179*, 1590–1608.
[59] J. Livet, T. A. Weissman, H. Kang, R. W. Draft, J. Lu, R. A. Bennis, J. R. Sanes, J. W. Lichtman, *Nature* **2007**, *450*, 56–62.
[60] L. Wei, Z. Chen, L. Shi, R. Long, A. V. Anzalone, L. Zhang, F. Hu, R. Yuste, V. W. Cornish, W. Min, *Nature* **2017**, *544*, 465–470.
[61] Y. Goltsev, N. Samusik, J. Kennedy-Darling, S. Bhate, M. Hale, G. Vazquez, S. Black, G. P. Nolan, *Cell* **2018**, *174*, 968–981.

Manuscript received: May 29, 2022
Accepted manuscript online: July 11, 2022
Version of record online: ■■, ■■

Research Articles

Protein Tags

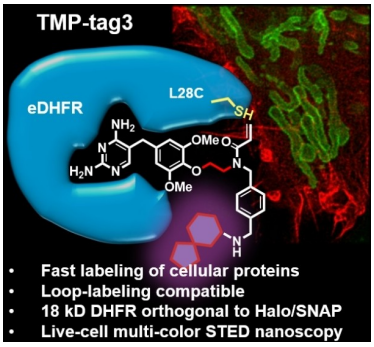

The third-generation TMP-tag3 is developed. It features optimized synthesis, fluorogenic labeling, and fast cellular intake. It performs well in comparative studies with HaloTag and SNAP-tag. The 18 kD-protein tag is compatible with loop insertion. The TMP-tag3 supplements and supplants the existing self-labeling protein tags, adding an orthogonal channel for multiplexed labeling and nanoscopic imaging.